Int. J. Radiation Oncology Biol. Phys., Vol. 46, No. 5, pp. 1329–1336, 2000

0360-3016/00/$–see front matter

PII S0360-3016(99)00353-3

PHYSICS CONTRIBUTION

A THEORETICAL STUDY OF CYLINDRICAL ULTRASOUND TRANSDUCERS FOR INTRACAVITARY HYPERTHERMIA

WIN-LI LIN, PH.D.,* WEN-CHANG FAN, M.S.,† JIA-YUSH YEN, PH.D.,†
YUNG-YAW CHEN, PH.D.,‡ AND MING-JIUM SHIEH, M.D.*

*Institute of Biomedical Engineering, and Departments of †Mechanical Engineering and ‡Electrical Engineering, National Taiwan University, Taipei, Taiwan

Purpose: The purpose of this paper was to examine the heating patterns and penetration depth when a cylindrical ultrasound transducer is employed for intracavitary hyperthermia treatments.
Methods and Materials: The present study employs a simulation program based on a simplified power deposition model for infinitely long cylindrical ultrasound transducers. The ultrasound power in the tissue is assumed to be exponentially attenuated according to the penetration depth of the ultrasound beam, and a uniform attenuation for the entire treatment region is also assumed. The distribution of specific absorption rate (SAR) ratio (the ratio of SAR for a point within the tissue to that for a specific point on the cavity surface) is used to determine the heating pattern for a set of given parameters. The parameters considered are the ultrasound attenuation in the tissue, the cavity size, and the transducer eccentricity.
Results: Simulation results show that the ultrasound attenuation in the tissue, the cavity size, and the transducer eccentricity are the most influential parameters for the distribution of SAR ratio. A low frequency transducer located in a large cavity can produce a much better penetration. The cavity size is the major parameter affecting the penetration depth for a small cavity size, such as interstitial hyperthermia. The heating pattern can also be dramatically changed by the transducer eccentricity and radiating sector. In addition, for a finite length of cylindrical transducer, lower SAR ratio appears in the regions near the applicator's edges.
Conclusion: The distribution of SAR ratio indicates the relationship between the treatable region and the parameters if an appropriate threshold of SAR ratio is taken. The findings of the present study comprehend whether or not a tumor is treatable, as well as select the optimal driving frequency, the appropriate cavity size, and the eccentricity of a cylindrical transducer for a specific treatment. **© 2000 Elsevier Science Inc.**

Cylindrical ultrasound transducer, Intracavitary hyperthermia, SAR ratio, Ultrasound attenuation, Transducer eccentricity, Cavity size.

INTRODUCTION

Diederich and Hynynen (1–3) examined the power deposition and temperature distribution for intracavitary ultrasound transducers with multi-element arrays. Segmenting the cylinders or sectors in the angular direction offers more control over the heating pattern. A complete intracavitary system with surface cooling water bolus has been constructed and is under clinical testing for the treatment of prostate (4), vaginal, and rectal tumors. The outside diameter of the cylinders was 1.0 or 1.5 cm, with a driving frequency 1.6 or 1.0 MHz. Diederich and Burdette (5) evaluated a tubular multitransducer applicator designed for transurethral ultrasound thermotherapy of prostate tissue. Their results show that ultrasound applicators have the potential to provide an improved spatial localization and control of the heating distribution over the existing transurethral thermal therapy techniques. Some investigators have also tried to design and evaluate the catheter-coupled tubular transducer devices (6–9) along with the design and the feasibility of direct-coupled tubular transducer applicators suitable for simultaneous interstitial hyperthermia and radiotherapy (10). Furthermore, Hand *et al*. (11) and Gavrilov *et al*. (12) have shown the possibility of focusing the ultrasound energy to a volume at a depth of 6 cm by simulation and phantom experiments. More advanced intracavitary ultrasound transducers with linear array applicators were developed and assessed by Hynynen, Hutchinson, and Buchanan *et al*. (13–15). The results of these transducers with more than 60 elements showed that practical intracavitary phased arrays are feasible and may significantly im-

Reprint requests to: Ming-Jium Shieh, M.D., Institute of Biomedical Engineering, College of Medicine, National Taiwan University, No. 1, Sec. 1, Jen-Ai Road, Taipei, Taiwan. Tel: (886) 223970800 ext. 1445; Fax: (886) 2 23940049; E-mail: kcju@ipmc.ee.ntu.edu.tw

Acknowledgments—The authors would like to thank the National Science Council and the Department of Health of the Republic of China for partially supporting this research under contract nos. NSC 87-2213-E-002-075 and DOH 87-HR-635, respectively.

Accepted for publication 6 August 1999.

prove the heating depth. In addition, Vrba *et al*. (16) indicated that the radial penetration of the specific absorption rate (SAR) for microwave antenna is limited by the radius of the cavity, and it is impossible to obtain a radial penetration larger than that of the cavity radius; whereas Sorbe *et al*. (17), Roos *et al*. (18), and Mandry *et al*. (19) have shown that the microwave antenna can be either centered in the outer casing or eccentrically positioned to achieve directed heating.

Cavity radius (R), transducer eccentricity (d) (the shifting distance between the central axes of the transducer and the cavity), and ultrasound attenuation (μ) in the tissue are the parameters which potentially affect the ultrasound energy deposition in the tissue around a cavity during an intracavitary hyperthermia. The present study employs a power deposition model for cylindrical ultrasound transducers to examine the relationship between the parameters and the distribution of SAR ratio in the tissue around the cavity. The results of this study presented herein are valuable for designing appropriate ultrasound heating probes for intracavitary hyperthermia and treatment planning.

METHODS AND MATERIALS

The deposition of ultrasound energy in the tissue around a cavity during an intracavitary hyperthermia is modeled as a cylindrical transducer, with uniform power that is emitted from the transducer face which penetrates into the tissue, as shown in Figs.1a and 1b. The radius of the transducer and the cavity is R_0, and R, respectively. The power output per unit length from the face of the transducer is Q. The central axis of the transducer is shifted to a distance (d: transducer eccentricity) away from that of the cavity along the x-axis. The polar coordinates (r,θ) for a new coordinate system o'-x'-y', adhering to the transducer central axis, is employed to describe the ultrasound power deposition in the tissue. The ultrasonic beam is presumed to be nondivergent in the longitudinal direction in the volume of interest, but radially diverging from the face of the transducer. The deposition of ultrasonic intensity at each cylindrical shell, with respect to the transducer central axis, is simplified as a uniform distribution to obtain a relatively simple approximation. Moreover, the ultrasound power in the tissue is assumed to be exponentially attenuated according to the penetration depth of the ultrasound beam. A uniform attenuation of ultrasound is assumed for the entire tissue as well.

One-dimensional (1D) power deposition

As the central axis of the transducer is coincident with that of the cavity (transducer eccentricity (d) = 0), the ultrasound power deposition in the tissue is one-dimensional (1D), and symmetrical to the central axis. The parameters for the power deposition are the ultrasound attenuation (μ) and the radius of the cavity (R). The ultrasound energy deposited on the surface of the cavity and in the tissue through a unit length of cylindrical shell with radius r is

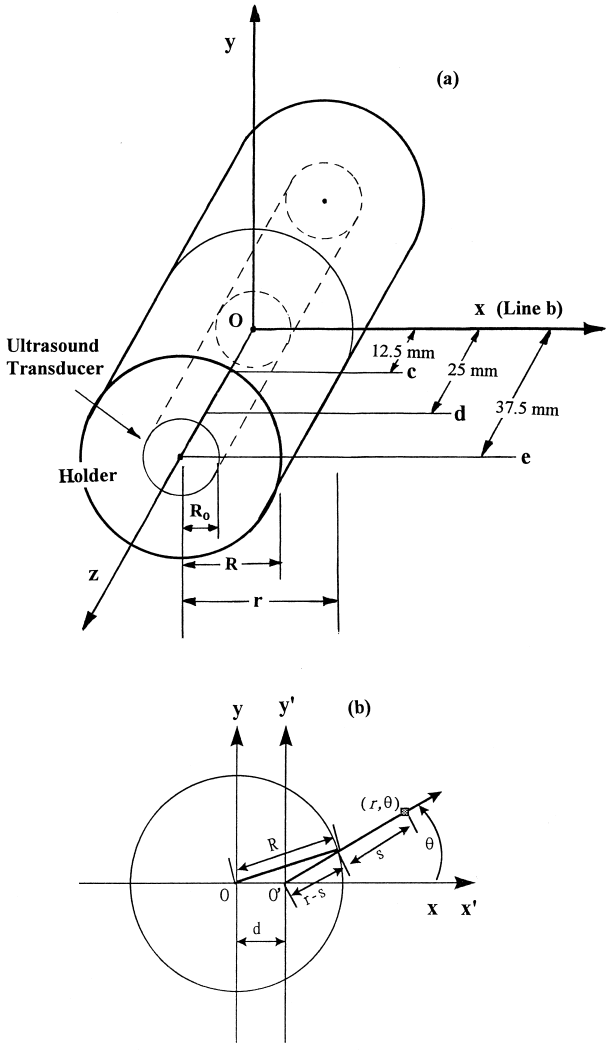

Fig. 1. (a) Schematic diagram of the geometry studied for the distributions of SAR ratio and temperature in the tissue when a cylindrical ultrasound transducer with a power Q emitted per unit length is placed within a cavity. Lines b, c, d, and e are located at 0.0, 12.5, 25.0, and 37.5 mm away from the transducer middle plane (o-x-y). (b) The relative position between the cylindrical transducer and the cavity. The central axis of the transducer is shifted to a distance (transducer eccentricity (d)) away from that of the cavity along the x-axis. The polar coordinates (r,θ) for the coordinate system o'-x'-y' is used to calculate the distribution of SAR ratio and the SAR value for the point $(R - d, 0^0)$ is taken as a reference for the present study.

$$Q(\mu, R; R) = Q \cdot e^{-2\mu_0(R-R_0)} \tag{1}$$

$$Q(\mu, R; r) = Q \cdot e^{-2\mu_0(R-R_0)} \cdot e^{-2\mu(r-R)} \tag{2}$$

where μ and μ_0 denote the ultrasound attenuations in the tissue and in the cooling water, respectively; whereas R and R_0 represent the radii of the cavity and the cylindrical ultrasound transducer under investigation, respectively; Q presents the ultrasound energy emitted from a unit length of the transducer surface, and $Q(\mu,R;r)$ denotes the ultrasound

energy deposited in a unit length of cylindrical shell with radius r.

The cylindrical ultrasound applicators are typically within a water bolus that can be expanded to fill or distend the body cavity. The attenuated ultrasound energy in the water (the region between R and R_0) is neglected due to negligible influence on the total energy changes, and the term $e^{-2\mu_0(R-R_0)}$ in Eqs. 1 and 2 can be eliminated. Hence, the ultrasound intensity on the cylindrical shell with radius r in the tissue is

$$I(\mu, R; r) = \frac{Q \cdot e^{-2\mu(r-R)}}{2\pi r} \tag{3}$$

And the ultrasound intensity on the surface of the cavity is

$$I(\mu, R; R) = \frac{Q}{2\pi R} \tag{4}$$

Assume that the ultrasound intensities are not large enough to cause wave distortion, and the attenuation and absorption coefficients of the tissue are equal (all of the attenuated energy is absorbed in the heating field) (20). The SAR in the homogeneous and uniformly attenuating media is then proportional to the ultrasound intensity. Thus, we can obtain the ratio of SAR on the cylindrical shell with radius r in the tissue to that on the surface of the cavity as

$$SR(\mu, R; r, R) = \frac{SAR(\mu, R; r)}{SAR(\mu, R; R)} = \frac{I(\mu, R; r)}{I(\mu, R; R)} = \frac{R}{r} \cdot e^{-2\mu(r-R)} \tag{5}$$

where $SR(\mu, R; r, R)$ is the SAR ratio of the cylindrical shell with radius r in the tissue to the surface of the cavity.

Two-dimensional (2D) power deposition

As the central axis of the transducer is shifted to a distance away from that of the cavity (transducer eccentricity (d) $\neq 0$), the ultrasound power deposition in the tissue is no longer symmetric in the angle dimension, and therefore becomes 2D. The parameters for the power deposition are the ultrasound attenuation in the tissue (μ), the radius of the cavity (R), and the eccentricity of the transducer (d). The polar coordinates (r,θ), with respect to the coordinate system o'-x'-y', are used to describe the power deposition in the tissue.

The power deposition for the point (r,θ) in the tissue is contributed by the ultrasound beam as shown in Fig. 1b. $S(R,d;r,\theta)$, the penetrating distance of the ultrasound beam into the tissue from the central axis of transducer to the point (r,θ), can be obtained by solving

$$R^2 = d^2 + (r - S)^2 + 2d(r - S)\cos\theta \tag{6}$$

The ultrasound intensity of the point (r,θ) in the tissue is

$$I(\mu, R, d; r, \theta) = \frac{Q \cdot e^{-2\mu S}}{2\pi r} \tag{7}$$

and the intensity of the point ($R - d$,0^0) on the surface of the cavity is

$$I(\mu, R, d; R - d, 0^0) = \frac{Q}{2\pi(R - d)} \tag{8}$$

The SAR ratio for the point (r,θ) in the tissue to the point ($R - d$, 0^0) on the surface of the cavity is

$$SR(\mu, R, d; r, \theta; R - d, 0^0) = \frac{SAR(\mu, R, d; r, \theta)}{SAR(\mu, R, d; R - d, 0^0)} = \frac{I(\mu, R, d; r, \theta)}{I(\mu, R, d; R - d, 0^0)} = \frac{R - d}{r} \cdot e^{-2\mu S} \tag{9}$$

where $SR(\mu, R, d; r, \theta; R - d, 0^0)$ is the SAR ratio of a point on the cylindrical shell with radius r in the tissue to the point ($R - d$, 0^0) on the surface of the cavity.

Temperature solver

To solve for the temperature distribution, Pennes' (21) steady-state bioheat transfer equation (BHTE) was used

$$-k\nabla^2 T + Wc_b(T - T_{ar}) = q \tag{10}$$

Where k and W denote the thermal conductivity and the blood perfusion of the tissue, respectively; T and T_{ar} represent the tissue and the arterial temperatures, respectively; c_b presents the specific heat of blood; and q denotes the absorbed ultrasonic power density.

The above BHTE is a simplification that neglects the effects of discrete blood vessels and the redistribution of thermal energy within the local vascular network. However, the BHTE is a good approximation that offers a practical approach for modeling biothermal processes (22–24) and performing general parameter studies. For convenience, this bioheat transfer equation can also be written in other forms (25, 26) to have a better description of the heat transfer in the tissue. We select the thermal properties to approximate averages for soft tissues (27–29). The thermal conductivity (k) is 0.5 (W m^{-1} $°C^{-1}$), the specific heat of blood (c_b) is 3,770 (J kg^{-1} $°C^{-1}$), and the arterial temperature (T_{ar}) is 37°C. The absorbed ultrasonic power density ($q = 2\,uI$) was obtained using the above procedure for a given power output per unit length (Q) from the transducer. All attenuated ultrasonic energy was assumed to be absorbed by the tissue in the heating region. The anatomic properties were assumed to remain constant throughout the entire field, and

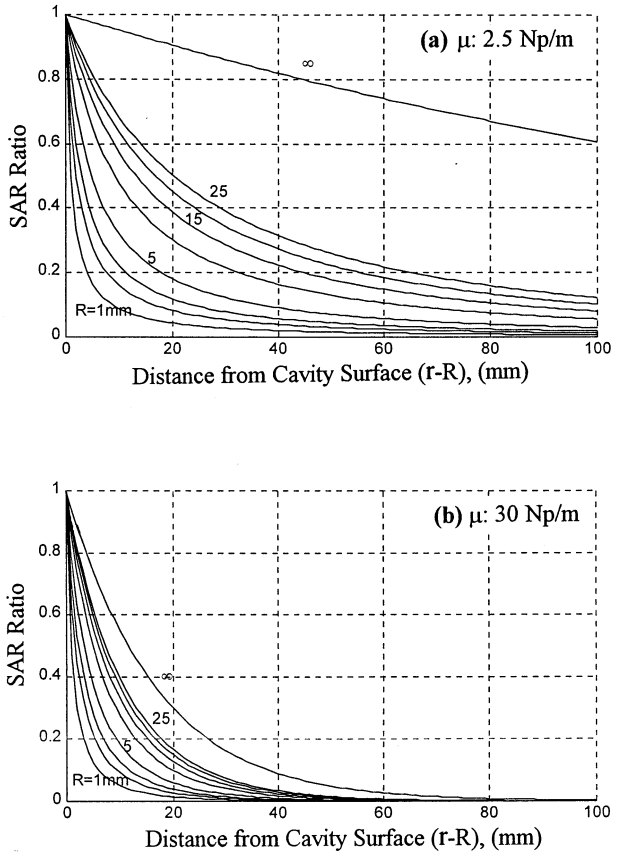

Fig. 2. The distributions of SAR ratio for the transducer eccentricity (d) equal to zero. The ultrasound attenuation (μ) in tissue varies from (a) 2.5 to (b) 30 Np m^{-1}, when the cavity radius (R) is 5, 10, 15, 20, 25, and ∞ mm, respectively.

metabolism was neglected due to its small contribution to the temperature changes (23, 30).

RESULTS

1D power deposition

To examine the effect of cavity size and ultrasound attenuation on the distribution of SAR ratio in the tissue when a cylindrical ultrasound transducer is used, the cavity radius (R) varies from 5, 10, 15, 20, 25, to ∞ mm, and the ultrasound attenuation (μ) from 2.5, 5, 10, 15, 20, to 30 Np m^{-1}. The central axis of the transducer is coincident with that of the cavity (transducer eccentricity (d) = 0); hence, the ultrasound power deposition in the tissue is 1D. Figures 2a and 2b present the distributions of SAR ratio in the tissue based on Eq. 5. These figures reveal that the SAR ratio for larger cavity (or lower attenuation) decreases from the surface of the cavity slower than that for smaller cavity (or higher attenuation). Figure 3 plots the depth of SAR ratio that equals to 0.5 based on Eq. 5. The figure shows that the depth of SAR ratio that equals to 0.5 is related to the attenuation and the size of the cavity. A larger cavity and/or a lower attenuation produce a larger depth of SAR ratio that equals to 0.5. This finding indicates that a lower attenuation

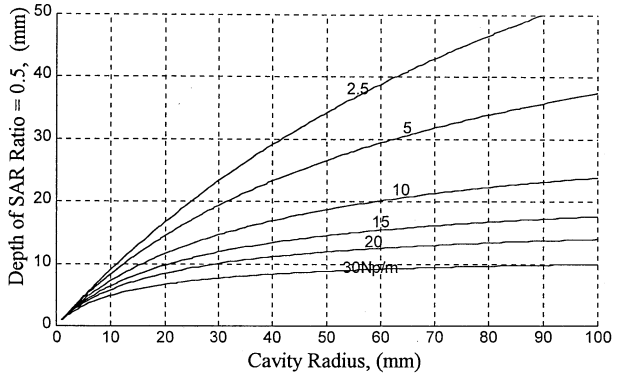

Fig. 3. Depth of the SAR ratio equal to 0.5 for different sizes of cavity and ultrasound attenuations, when the transducer eccentricity (d) is equal to zero.

with a larger cavity has a better penetration. Figures 2a, 2b, and 3 depict the relationship between the treatable region and the attenuation for different sizes of cavity if an appropriate threshold of SAR ratio is taken. For instance, we might define the domain with SAR ratio higher than 0.5 as the treatable region. Thus, the above results indicate that the domain of treatable region depends on the attenuation and the cavity size. Therefore, a lower attenuation with a larger cavity produces a deeper treatable domain, while higher attenuations can be used in the superficial treatment of the cavity. These figures display the treatable domain for a given cavity size and attenuation. Thus, restating the cavity size and the attenuation can determine the treatable domain. The results are presented in terms of tissues with different acoustic attenuation properties. Once the attenuation coefficient of the treatment tissue is known, an appropriate driving frequency can be obtained. For example, an attenuation coefficient of 5 Np m^{-1} MHz^{-1} is approximate for soft tissue (for most soft tissues and tumors, the attenuation coefficient ranges between 4 and 15 Np m^{-1} MHz^{-1} [31, 32]) and then the range of 2.5–30 Np m^{-1} covers an approximate frequency range of 0.5–6.0 MHz. Hence, the above finding suggests that the treatable portion can be determined by selecting an appropriate cavity size and driving frequency.

2D power deposition and temperature distribution

As the central axis of cylindrical transducer is shifted to a distance away from that of the cavity (transducer eccentricity (d) $\neq$ 0), the ultrasound power deposition in the tissue becomes 2D. The ultrasound attenuation (μ), cavity radius (R), and transducer eccentricity (d) are the factors which potentially affect the distribution of SAR ratio. Figures 4a–d display the 2D distributions of SAR ratio based on Eq. 9 for an ultrasound attenuation of 2.5 Np m^{-1}, cavity radius of 20 mm, and transducer radius of 5 mm, while the transducer eccentricity (d) varied from 0, 5, 10 to 15 mm, respectively. The figures indicate that the distribution of SAR ratio dramatically changes with the transducer eccentricity. Figures 4e–h show the temperature distributions

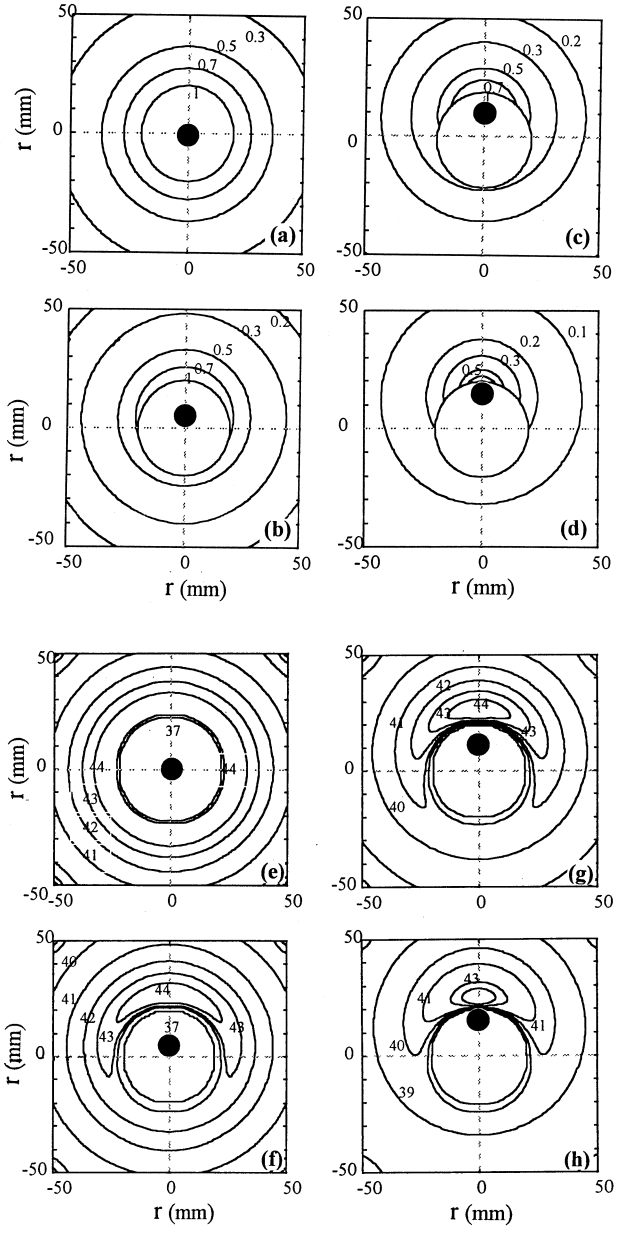

Fig. 4. (a–d) Distributions of SAR ratio for a cylindrical transducer with 2.5 Np m^{-1} attenuation (μ) and a 20-mm cavity radius (R). The transducer eccentricity (d) is 0, 5, 10, and 15 mm, respectively. (e–h) Temperature distributions for (a–d), respectively. The applicator OD and position are shown by a solid circle, while the innermost circle with a radius of 20 mm is the cavity wall, and also represents the 37°C isoline for the temperature plots.

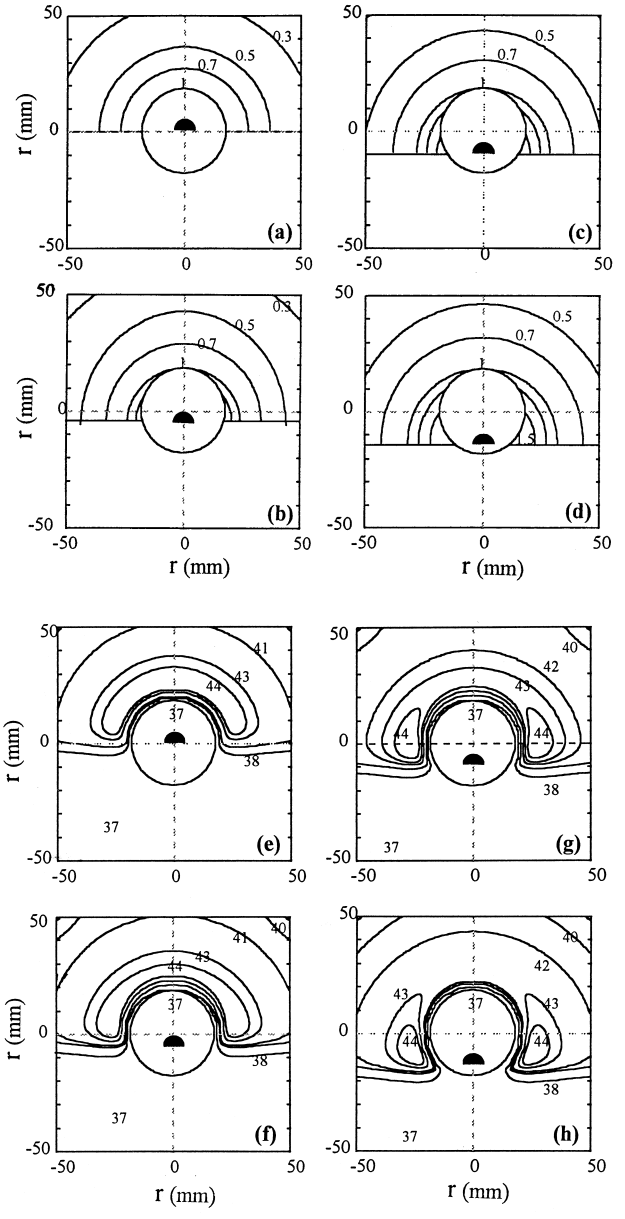

Fig. 5. (a–d) show the distributions of SAR ratio for a half-cylindrical transducer with 2.5 Np m^{-1} attenuation (μ) and a 20-mm cavity radius (R), while the transducer eccentricity (d) from the back direction is 0, 5, 10, and 15 mm, respectively. (e–h) Temperature distributions for (a–d), respectively. The applicator OD and position are shown by a half solid circle, while the innermost circle with a radius of 20 mm is the cavity wall, and also represents the 37°C isoline for the temperature plots.

corresponding to the SAR ratio in Figs. 4a–d, respectively. The temperature of the cavity surface is set at 37°C and the maximum tissue temperature is maintained at 45°C, while a uniform blood perfusion (6 kg m^{-3} s^{-1}) is assumed for the entire simulated tissue. These figures display that the transducer eccentricity provides a directional heating and the region of SAR ratio higher than 0.5 is controlled by the eccentricity.

When a half-cylindrical transducer is employed, the SAR ratio on the back of the transducer is zero due to the collimated and radially diverging ultrasound beam. Because the eccentricity of the half-cylindrical transducer is varied, the SAR ratio distribution in the tissue in front of the transducer may be influenced by the eccentricity of the transducer. Figures 5a–d present the distributions of SAR ratio in the tissue when a half-cylindrical transducer with the above characteristics is employed, while the transducer eccentricity from the back direction is 0, 5, 10, and 15 mm, respectively. Figures 5e–h show the temperature distributions corresponding to the SAR ratio for Figs. 5a–d, respec-

tively. The temperature of the cavity surface is set at 37°C and the maximum tissue temperature is maintained at 45°C, while a uniform blood perfusion (6 kg m^{-3} s^{-1}) is assumed for the entire simulated tissue. The results show that the region with high SAR ratio and temperature, shifts to the corner as shown in Figs. 5d and 5h, which may overcome the SAR dips and a stronger thermal conduction in the corner region for a half-cylindrical transducer. The results also indicate that a half-cylindrical transducer with eccentricity can cause a much larger directional heating.

Figures 4 and 5 reveal that the desired treatment region can be determined by selecting an appropriate radiating sector and positioning the cylindrical ultrasound transducer with a proper eccentricity. These results also indicate that a potential heating problem (one side preferentially heated while the opposite side is underheated) may occur when a symmetric heating is desired while the intracavitary transducer is not centered in the cavity.

The above results show that: (a) the cavity size, transducer eccentricity, ultrasound attenuation in the tissue, and transducer active sector are the most influential factors for the SAR ratio distributions (or the heating patterns); (b) high driving frequencies should be used for heating the region close to the cavity surface, and low frequencies for deeper and larger regions; (c) the SAR ratio distribution also depends on the cavity size; a larger cavity has a slower decay of SAR ratio and hence results in a better penetration; (d) the transducer eccentricity can create a high SAR ratio region close to the transducer; and (e) the eccentricity of a half-cylindrical transducer can create a larger region with a high and rather uniform SAR ratio in front of the transducer face.

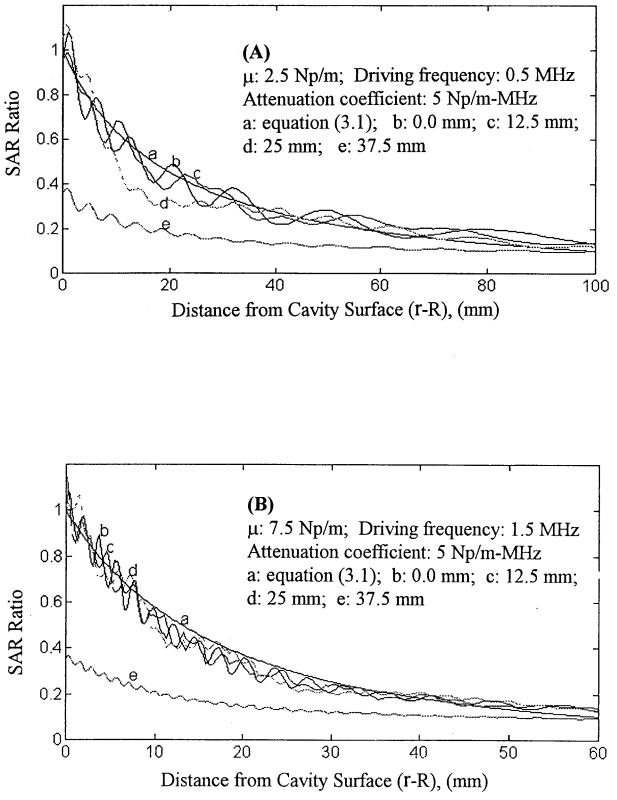

Fig. 6. Distribution of SAR ratio in the radial direction for theoretical wave equation and the simplified model of a cylindrical ultrasound transducer with a length of 75 mm and a radius of 5 mm is placed in a 20-mm cavity radius (R). The SAR ratio distributions are for the radial lines located at 0, 12.5, 25, and 37.5 mm away from the middle plane of the transducer (see Fig. 1a).

DISCUSSION

The 1D and 2D simulations assume a long tube transducer that neglects the edges. However, the SAR ratio distribution close to the extreme edges of the transducer is different, because the portion of the transducer contributing to the ultrasound power deposition is related to the position. Hence, it is necessary to investigate the effect of extreme edges on the SAR ratio distribution. Figures 6a and b show the distributions of normalized ultrasound intensity calculated using the proposed model and the numerical solution of the wave equation (33, 34) for a cylindrical transducer with a radius of 5 mm, length of 75 mm, and a driving frequency of 0.5 and 1.5 MHz, respectively. The cavity radius is 20 mm and ultrasound attenuation coefficient in the tissue is assumed to be 5.0 Np m^{-1} MHz^{-1}. Lines b, c, d, and e are the distributions of normalized ultrasound intensity in the radial direction beginning from the surface of the cavity and located 0.0, 12.5, 25.0, and 37.5 mm away from the transducer's middle plane, respectively (see Fig. 1a). The solid line (line a) with an exponential decay, taken from Fig. 2a with cavity radius 20 mm, is used to compare the difference in power intensities between the proposed model and the numerical solution of the theoretical wave equation (33, 34) for different locations. These figures indicate that the distributions of SAR ratio for the proposed model is quite adhesive to the theoretical field except to the one at extreme edges of the transducer. This is due to the contributed portion of the transducer to the power intensity field is decreased in the region closer to the extreme edges of the transducer. This exponential model has been experimentally verified by Diederich *et al.* (2) using an ultrasound applicator with a driving frequency of 1.6 MHz in degassed water; whereas the 1D and 2D simulations assume a long tube transducer and neglect the edges. However, using an array of multiple ultrasound transducers with only a few millimeters between the transducer segments, thermal smearing fills in wherever there are dips in the SAR distribution between the elements (1).

The SAR ratio distribution and the cooling water temperature are the two major factors by which the temperature distribution can be controlled during the intracavitary hyperthermia. The influence of the cooling water on the heating depth is about 1 cm (2, 35), whereas the transducer can form different patterns of the SAR ratio distribution by selecting the transducer eccentricity, the cavity size, and the driving frequency. A lower frequency transducer with a larger cavity can produce a deeper penetration by which a

thicker tumor in the radial direction can be treated. The temperature close to the cavity surface is mainly controlled by the cooling water, either by the temperature or the flow rate of the water (18). A higher cooling water temperature results in a treatment boundary closer to the cavity surface. The temperature at greater distances from the cavity surface is mainly determined by the level of the ultrasound power applied. Because the influence of the cooling water is limited to about 1 cm in the radial direction, the present study focuses on the SAR ratio distributions related to the parameters which can be employed in the transducer design to achieve the desired heating patterns.

The study covers a range of cavity radius from 1 to 25 mm, and also considers the limitation case ∞ mm (planar transducer). The results can be used for both interstitial and intracavitary treatments. However, for interstitial treatments, the penetration depth can be improved by using a maximum acceptable invasive radius of the implanted catheter (see Fig. 3). The effect of the driving frequency on the penetration depth for the interstitial treatments is not very significant (36); however, the selection of driving frequency requires to meet the relationship between the catheter size and the thickness of the transducer wall; whereas for intracavitary treatments, the vagina and rectum are the suitable regions, while the cervix uteri and esophagus are secondary. In addition, further study of SAR ratio and temperature distributions for the esophagus heating is necessary due to the high ultrasound absorption on the esophagus wall.

The allowable cavity size, desired heating depth in the radial direction, and ultrasound attenuation coefficient in the tissue are the three basic data required when designing an appropriate cylindrical ultrasound transducer for a specific treatment. Because the allowable cavity size and the desired heating depth are known, an appropriate ultrasound attenuation, which is related to the desired driving frequency, can be obtained in Fig. 3. Once the desired frequency is determined, the active portion of the cylindrical transducer (360°, 180°, or others) and/or the transducer eccentricity can be selected according to Figs. 4 and 5.

CONCLUSION

The study employs a simplified model of ultrasound power deposition to investigate the effects of cavity size, transducer eccentricity, active sector, and driving frequency of the transducer on the distributions of SAR ratio and temperature for a cylindrical transducer located within a cavity. In addition, for a specific treatment, an appropriate driving frequency, transducer eccentricity, and active sector, and the cooling water temperature can be determined as long as the cavity size, treatment region boundary and ultrasound attenuation coefficient in the tissue are known. The findings of this study can be then used as a guideline to (a) determine if the desired treatment region is treatable, and (b) select a proper driving frequency for the transducer, and an appropriate transducer eccentricity for a treatment when the desired treatment region is known during the clinical treatment. These SAR ratio patterns are the initial results that could then be modified for additional modeling that would include the arrangement of transducer elements, temperature calculations, power control of each element to meet the blood perfusion fluctuation, etc.

REFERENCES

1. Diederich C, Hynynen K. The development of intracavitary ultrasonic applicators for hyperthermia: A theoretical and experimental study. *Med Phys* 1990;17:626–634.
2. Diederich C, Hynynen K. Induction of hyperthermia using an intracavitary multielement ultrasonic applicator. *IEEE Trans Biomed Eng* 1989;36:432–438.
3. Diederich C, Hynynen K. The feasibility of using electrically focused ultrasound arrays to induce deep hyperthermia via body cavities. *IEEE Trans Ultrasonics Ferroelec Freq Contr* 1991;38:207–219.
4. Fosmire H, Hynynen K, Drach GW, *et al.* Feasibility and toxicity of transrectal ultrasound hyperthermia in the treatment of locally-advanced denocarcinoma of the prostate. *Int J Radiat Oncol Biol Phys* 1993;26:253–259.
5. Diederich CJ, Burdette EC. Transurethral ultrasound array for prostate thermal therapy: Initial studies. *IEEE Trans Ultrasonics Ferroelec Freq Contr* 1996;43:1011–1022.
6. Hynynen K. The feasibility of interstitial ultrasound hyperthermia. *Med Phys* 1992;19:979–987.
7. Diederich CJ, Stauffer PR, Sneed PK, *et al.* The design of ultrasound applicators for interstitial hyperthermia. Proceedings of the IEEE Ultrasonics Symposium, 1993. p. 1215–1219.
8. Hynynen K, Davis KL. Small cylindrical ultrasound sources for induction of hyperthermia via body cavities. *Int J Hyperthermia* 1993;9:263–274.
9. Diederich CJ. Ultrasound applicators with integrated catheter-cooling for interstitial hyperthermia: Theory and preliminary experiments. *Int J Hyperthermia* 1996;12:279–297.
10. Diederich CJ, Khalil IS, Stauffer PR, *et al.* Direct-coupled interstitial ultrasound applicators for simultaneous thermobrachytherapy: A feasibility study. *Int J Hyperthermia* 1996; 12:401–419.
11. Hand JW, Ebbini E, O'Keefe D, *et al.* An ultrasound linear phased array for use in intracavitary applicators for thermotherapy of prostatic diseases. Proceedings of the IEEE Ultrasonics Symposium, 1993. p. 1225–1228.
12. Gavrilov LR, Hand JW, Abel PD. Ultrasound transrectal linear phased array for thermotherapy of prostatic diseases. Proceedings of the 7th International Congress on Hyperthermic Oncology, Roma, Italy, 1996. Vol. II, p. 399–401.
13. Buchanan MT, Hynynen K. The design and evaluation of an intracavitary ultrasound phased array for hyperthermia. *IEEE Trans Biomed Eng* 1994;41:1178–1187.
14. Hutchinson EB, Buchanan MT, Hynynen K. Design and optimization of an aperiodic ultrasound phased array for prostate thermal therapies. *Med Phys* 1996;23:767–776.
15. Hutchinson EB, Hynynen K. Intracavitary ultrasound phased arrays for noninvasive prostate surgery. *IEEE Trans Ultrasonics Ferroelec Freq Contr* 1996;43:1032–1042.
16. Vrba J, Franconi C, Lapes M. Theoretical limits for the penetration depth of intracavitary applicators. *Int J Hyperthermia* 1996;12:737–742.
17. Sorbe B, Roos D, Karlsson L. The use of microwave-induced

hyperthermia in conjunction with afterloading irradiation of vaginal carcinoma. *Acta Oncol* 1990;29:1029–1033.
18. Roos D, Seegenschmiedt MH, Klautke G, *et al.* A new microwave applicator with integrated cooling system for intracavitary hyperthermia of vaginal carcinoma. *Int J Hyperthermia* 1996;12:743–756.
19. Manry C, Brochat S, Chou CK, *et al.* An eccentrically coated asymmetric antenna applicator for intracavitary hyperthermia treatment of cancer. *IEEE Trans Biomed Eng* 1992;39:935–942.
20. Hynynen K. Biophysics and technology of ultrasound hyperthermia. In: Gautherie M, editor. Method of external hyperthermic heating. Berlin: Springer-Verlag; 1990. p. 61–116.
21. Pennes HH. Analysis of tissue and arterial blood temperatures in the resting human forearm. *J Appl Phys* 1948;1:93–122.
22. Arkin H, Xu X, Holmes KR. Recent developments in modeling heat transfer in blood perfusion tissues. *IEEE Trans Biomed Eng* 1994;41:97–107.
23. Roemer RB. Thermal dosimetry. In: Gautherie M, editor. Thermal dosimetry planning. Berlin: Springer-Verlag; 1990. p. 119–214.
24. Chato JC. Fundamentals of bioheat transfer. In: Gautherie M, editor. Thermal dosimetry planning. Berlin: Springer-Verlag; 1990. p. 1–56.
25. Nyborg WL. Solutions of the bioheat transfer equation. *Phys Med Biol* 1988;33:785–792.
26. NCRP Report No. 113. Exposure criteria for medical diagnotics ultrasound: I. Criteria based on the thermal mechanisms. Bethesda, MD: NCRP Publication; 1992. p. 52–60.
27. Bowman HF. Heat transfer mechanism and thermal dosimetry. *J Natl Cancer Inst Monogr* 1981;61:437–445.
28. Chato JC. Selected thermophysical properties of biological materials. In: Shitzer A, Eberhart RC, editors. Heat transfer in medicine and biology, analysis and applications. New York: Plenum; 1985. p. 413–418.
29. Gordon RG, Roemer RB, Horvath SM. A mathematical model of the human temperature regulatory system - transient cold exposure response. *IEEE Trans Biomed Eng* 1976;23:434–444.
30. Jain RK. Bioheat transfer: Mathematical models of thermal systems. In: Storm FK, editor. Hyperthermia cancer therapy. Boston: Hall; 1983. p. 9–46.
31. Goss SA, Frizzell LA, Dunn F. Ultrasonic absorption and attenuation in mammalian tissues. *Ultrasound Med Biol* 1979; 5:181–186.
32. Goss SA, Johnston RL, Dunn F. Comprehensive compilation of empirical ultrasonic properties of mammalian tissues. *J Acoust Soc Am* 1978;64:423–457.
33. Zemanek J. Beam behavior within the nearfield of a vibrating piston. *J Acoust Soc Am* 1971;49:181–191.
34. Morse PM, Ingard KU. Theoretical acoustics. New York: McGraw-Hill; 1968.
35. Lin W-L, Yen J-Y, Chen Y-Y, *et al.* Relationship between acoustic aperture size and tumor conditions for external ultrasound hyperthermia. *Med Phys* 1999;26:818–824.
36. Jarosz BJ, Kaytar D. Ultrasonic waveguide applicator arrays for interstitial heating: A model study. *IEEE Trans Ultrasonics Ferroelec Freq Contr* 1998;45:806–814.